Short communication

Crustal motion along the Calabro-Peloritano Arc as imaged by twelve years of measurements on a dense GPS network

Mario Mattia [a], Mimmo Palano [a,*], Valentina Bruno [a,b], Flavio Cannavò [a]

[a] Istituto Nazionale di Geofisica e Vulcanologia, Sezione di Catania, P.zza Roma, 2, 95123 Catania (Italy)
[b] Università degli Studi di Catania, Dipartimento di Scienze Geologiche, Corso Italia 57, 95129 Catania (Italy)

ARTICLE INFO

ABSTRACT

In this work, we show the results of 12 years of continuous and survey-mode GPS measurements carried out along the western part of the Calabro-Peloritano Arc, from 1996 until the more recent acquisitions in 2008. The results highlight that a NW–SE-oriented ~0.15 μstrain/yr extension across the Messina Strait and the Aeolian–Tindari–Letojanni fault system is active. Moreover, a N–S compressive strain-rate (~0.65 μstrain/yr) is acting across Vulcano and Lipari Islands coupled with an extensional strain-rate of ~0.15 μstrain/yr in the E–W direction. Finally, taking into account the observed horizontal velocity field, an analytical inversion was performed to obtain a reliable model of deformation of the investigated area. The main results are consistent both with focal mechanism solutions and the current structural setting of the investigated area.

© 2009 Elsevier B.V. All rights reserved.

1. Introduction

On December 28 1908, a Mw = 7.1 earthquake struck the cities of Messina and Reggio Calabria (southern Italy) causing more than 100 000 casualties. Since that dramatic event, geologists and geophysicists have attempted to understand the complex tectonics of the Calabro-Peloritano Arc, with the aim of improving the knowledge on the current geodynamic setting of this area and in particular on the rate and the shape of inter-seismic loading of active faults cutting the area. Notwithstanding geodetic studies of this area began as early as the 1970s, knowledge of the crustal deformation pattern is still far from satisfactory since all published data have a limited areal coverage (*e.g.* Anzidei et al., 1998; Bonaccorso, 2002) or poor spatial densities (*e.g.* Hollenstein et al., 2003; D'Agostino and Selvaggi, 2004; Serpelloni et al., 2005).

In this work, in order to obtain a detailed spatial resolution of the ongoing crustal motion, we analyzed periodical and continuous GPS data collected between 1996.00 and 2008.21 on three geodetic networks installed in the Peloritani Mts., on the Aeolian Islands and across the Messina Strait (Fig. 1a,b). In the following, we present and discuss the main results, in terms of i) velocity field (computed in an Eurasian reference frame) and ii) strain-rate field of the investigated area. Finally, we apply different approaches (*i.e.* vectorial decomposition of velocities measured across the faults; analytical inversion of

velocity field) to our results, in order to verify their coherence with geological evidences and models proposed in literature. In particular, we have found that the observed deformation pattern is influenced by local tectonics, although the NNW–SSE regional compression related to the Nubia–Eurasia interaction is the main "engine" of the kinematic of this area.

2. Background setting

The present-day tectonic framework of northern Sicily and southern Calabria is the result of the geodynamic processes due to the Neogene–Quaternary convergence between Nubia and Eurasia (*e.g.* Barberi et al., 1973; Patacca et al., 1990) and to the subduction and rollback of the Ionian plate underneath the Calabria and the Tyrrhenian Sea (*e.g.* Malinverno and Ryan, 1986; Gueguen et al., 1998; Faccenna et al., 2001; Gvirtzman and Nur, 2001). The tectonic setting of this area is dominated by two main systems: the "Messina Strait" (hereinafter MS) and the Aeolian–Tindari–Letojanni fault system (hereinafter ATL; Fig. 1a,b). The former, developed in north-eastern Sicily and southern Calabria, describes a continuous extensional belt cutting at high-angle the front of the Calabro-Peloritano Arc (Tortorici et al., 1995). It is characterized by faults with steeply inclined surfaces (dip ≥ 70°) and showing prevailing dip–slip movements.

The latter, developed between northern Sicily and the southernmost part of the Aeolian Archipelago, is generally characterized by steeply inclined scarps (dip ≥ 60°) that mostly dip eastward. Structural studies carried out along the Lipari–Vulcano complex revealed how this fault system is arranged with an en-echelon configuration

* Corresponding author. Tel.: +39 095 7165800; fax: +39 095 435801.
E-mail address: palano@ct.ingv.it (M. Palano).

along two main branches, N160°E-oriented, bordering the western and the eastern flanks of Vulcano and is characterized by prevailing right-lateral strike–slip movements (*e.g.* Barberi et al., 1994; Ventura, 1994; De Astis et al., 2003). In the northern margin of Sicily, the fault system is characterized by an early kinematics as a right-lateral fault during Pliocene age, followed by dominant normal mechanism in Quaternary age (*e.g.* Ghisetti and Vezzani, 1982). Since 1983, more than 2500 crustal earthquakes with $M_{max} = 4.4$ have been recorded in the investigated area (ftp://ftp.ingv.it/pro/bollet). In the southern Tyrrhenian Sea, the depth distribution of earthquakes, as deep as 600 km, fairly well depicts a subvertical slab extending from Calabria to the southern Tyrrhenian Sea (Selvaggi and Chiarabba, 1995). Seismicity occurring along the slab shows focal mechanisms with pervasive down–dip compression at all depths beneath 100 km, while seismicity occurring at shallow depth has normal faulting focal mechanisms evidencing a general extension of the area (Selvaggi, 2001; Neri et al., 2005). Deep and intermediate earthquakes abruptly terminate westward beneath northern Sicily and the Aeolian Archipelago, whereas shallower seismicity (depth range 0–25 km) has a clear NNW–SSE trend matching well with the ATL (Neri et al., 2005). Focal mechanisms computed for this area reveal normal faulting coupled with dextral transcurrence. Westward of the ATL, the seismic events mostly occur in the upper 30 km of the crust, showing a spatial distribution along an E–W trend and having focal mechanisms with NNW–SSE and NW–SE compressive axes (Fig. 1a; Frepoli and Amato, 2000; Neri et al., 2003, 2005; Pondrelli et al., 2006) in agreement with a NW–SE compression inferred by large-scale GPS networks (Hollenstein et al., 2003; Serpelloni et al., 2005; Ferranti et al., 2008a) and with the main NNW–SSE plate convergence predicted for this area by large-scale crustal motion models (Sella et al., 2002; Nocquet and Calais, 2004). Despite the absence of any active fault mapped here (Valensise and Pantosti, 2001), the focal mechanisms distribution indicates that thrust or reverse faults could be activated offshore from the northern Sicily coast in future.

All these features clearly show that two main crustal domains along the Calabro-Peloritano Arc can be recognized: a contractional domain in the north-western sicilian offshore and an extensional domain in north-eastern Sicily and southern Calabria. The transition between the two domains seems to occur along the ATL fault system.

3. Geodetic network and data processing

GPS monitoring of the ground deformations of Peloritani–Nebrodi area (Fig. 1b) started in late 1995, when a geodetic network was set up. The network, surveyed for the first time in October 1996, consisted of 7 benchmarks and has been successively expanded to reach the current configuration of 12 benchmarks. In late 2000, a geodetic network of 13 benchmarks was established across the Messina Strait and was surveyed for the first time in February 2001 (Mattia et al., 2006). In the framework of the Italian National GPS Network RING (http://ring.gm.ingv.it/), since early 2005, the "Istituto Nazionale di Geofisica e Vulcanologia" has installed 5 CGPS stations thereby improving the spatial detail of the entire north-eastern Sicily and southern Calabria areas (Table 1). All non-permanent and CGPS data collected between 1996.00 and 2008.21, together with 9 continuously operating IGS stations (AJAC, CAGL, GRAS, GRAZ, LAMP, MATE, MEDI, NOT1 and NOTO), were analysed using the GAMIT/GLOBK software (Herring et al., 2006a,b) with IGS precise ephemerides and Earth orientation parameters (http://www.iers.org) to produce loosely constrained daily solutions. By using the GLOBK Kalman filter, these solutions were combined, on a daily basis, with global solutions (IGS1, IGS2, IGS3, IGS4 and EURA) provided by the SOPAC (ftp://garner.ucsd.edu/pub/hfiles) and local solutions of data collected on the Aeolian Archipelago and analyzed in Mattia et al. (2008a), in order to create a daily unconstrained combined network solution. By using the GLORG

module of GLOBK (Herring et al., 2006b) the solutions were transformed into the ITRF2005 reference frame and then rotated into a fixed Eurasian frame (Altamimi et al., 2007).

4. Data analyses

4.1. GPS velocity field

GPS velocity field in the Eurasian reference frame for the investigated area is reported in Fig. 1b. Velocities observed at CGPS stations have been determined from data spanning ~2.5 years (MMME, MILA, MRSU and MESS). As postulated by some authors (Blewitt and Lavallee, 2002) and as testified by the spatial consistency of the velocity field and the similarity in velocities from nearby GPS sites with longer observation intervals (*e.g.* PACE, MM01 and MM04; Fig. 1d), this limited time span can be considered sufficient for considerations on tectonic aspects. A striking aspect of the ground deformation pattern is a marked decrease of velocity values from northern Sicily to the Aeolian Islands, highlighting how part of the NNW–SSE regional compression is localized within a ~15 km-wide zone with the buttressing of Vulcano and Lipari islands. In particular, as shown along a roughly N–S profile (Fig. 1b), the velocity values pass from ~7.5 mm/yr in the northern part of Sicily (*e.g.* CALA, MONT, TIND) to ~10.5 mm/yr in the southern part of Vulcano Island (*e.g.* VSAR, VSER and VMOL; Fig. 1c), to ~5.4 mm/yr in the central part of Lipari Island (*e.g.* LMAZ and LROS), to ~2.9 mm/yr on Stromboli Island (*e.g.* SPLN and STDF). In addition, in northern Sicily and southern Calabria, going from west toward east the velocity field is characterized by a progressive rotation from an azimuth of ~N15°W to an azimuth of ~N15°E. This aspect is coupled with a slight decrease of velocity values in an eastward direction. Along the Vulcano–Lipari–Stromboli axis, the velocity field is characterized by a rotation from an azimuth of ~N10°W on Vulcano and Lipari islands to an azimuth of ~N12°E on Stromboli Island. It is noteworthy that the velocities of the Vulcano (with the exception of VCRA), Lipari and Stromboli islands can be considered unaffected by volcanic effects (Mattia et al., 2008a, b), while the velocities of Panarea Island may certainly be biased by local effects due to fractures and geothermal effects (D'Agostino and Selvaggi, 2004; Esposito, 2007). For these reasons, the velocities of the stations PANA and LI3D (Panarea and Lisca Bianca Islands) haven't been considered in the profile reported in Fig. 1e.

4.2. Strain-rate field

Taking into account the network geometry and the estimated velocity at each site, we calculated the horizontal strain-rate field, applying the method of Haines and Holt (1993). Following this method, we adopted a spherical geometry, expressed in terms of a rotation function $W(r)$ by using a bi-cubic Bessel interpolation on a curvilinear grid (Haines et al., 1998) with a variable spacing of knots. The estimated strain-rate distributions are shown in Fig. 2a,b,c as principal axes, dilatation, and maximum shear. The principal axes of strain-rate clearly detect an area of prevailing N–S shortening (about 0.65 μstrain/yr), coupled with an E–W extension (about 0.15 μstrain/yr) between Vulcano and Lipari islands. In addition, a NNE–SSW shortening of about 0.1 μstrain/yr can be recognized between Stromboli and Lipari islands. Across the Nebrodi–Peloritani and the Messina Strait areas the strain-rate pattern is extensional, showing maximum values (about 0.15 μstrain/yr) along the MS fault system (with principal axes mostly NW–SE–oriented) and the ATL fault (with principal axes NW–SE-oriented). This pattern is confirmed by the dilatation strain-rate distribution (Fig. 2b). Regarding the maximum shear strain-rate, the greatest values (about 0.75 μstrain/yr) are detected between Vulcano and Lipari islands, and lower values are distributed over the whole investigated area (Fig. 2c).
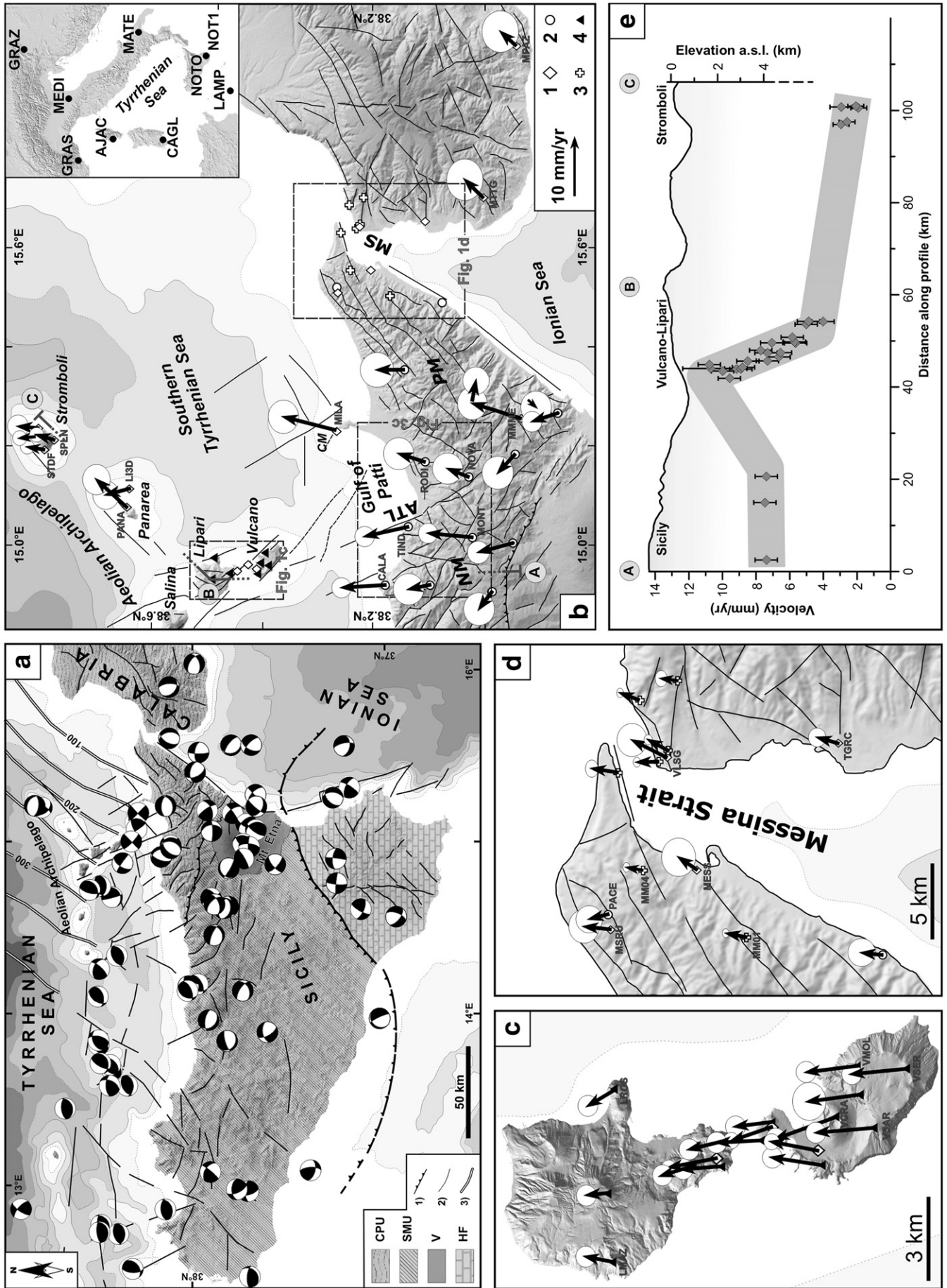
4.3. Estimation of active deformation across the ATL and MS faults system

The horizontal parallel and perpendicular movement rates of the ATL and the MS faults system were estimated by using a statistical approach applied to a vectorial decomposition of the velocities of stations located across the ATL and the MS faults system. In particular for each pair of stations located across a specific fault, we resolved the rates of parallel (*i.e.* strike–slip) and perpendicular (*i.e.* tensile or opening) movement. Starting from these values, the average values and the standard deviations were estimated.

Considering a N40°W trend for the Aeolian sector of the ATL fault system, and the network configuration as reported in Fig. 3a, we estimated a right-lateral strike–slip of 1.6 ± 1.4 mm/yr and a tensile component of -2.5 ± 1.1 mm/yr. On the sicilian sector, the ATL shows different orientations passing from about N30°W (close to TIND) to about N50°W (close to NOVA) (Billi et al., 2006; Giammanco et al., 2008). Because TIND is located on the foot-wall of ATL whereas NOVA is located on his hanging-wall, we resolved the rates of parallel and perpendicular movement on a fault N35°W-trending. In particular, considering the network configuration as reported in Fig. 3b, we estimated a dextral strike–slip of 3.9 ± 0.6 mm/yr and a tensile component of 1.4 ± 0.6 mm/yr. Since the Messina Strait area is cut by several tectonic sources (*i.e.* Scilla fault; Armo fault, Reggio Calabria fault, Messina fault; see Ferranti et al., 2008b for an overview) and because our network geometry is centred around the strait, we prefer performing the computation along the N30°E trends, *i.e.* parallel to the strait, rather than estimate strike–slip and opening components on a specific fault. Main results indicate a left strike–slip of 0.4 ± 1.1 mm/yr and a tensile component of 0.5 ± 0.8 mm/yr (Fig. 3c).

This approach showed how the deformation pattern may surely be considered as the result of the interaction between the main NNW–SSE regional compression and the local movements of the faults cutting the overall investigated area. This approach is able to well describe the style of deformation along the ATL fault system; however, it fails to describe the style of deformation occurring in the Messina Strait area, where the high errors associated to strike–slip and tensile components and the highly scattered rose diagram (Fig. 3c) confirm how the deformation in this area is more complex. In the following, we performed an analytical inversion taking into account the observed horizontal velocity field in order to obtain a reliable model of deformation of the investigated area.

4.4. Modelling of ground deformation pattern

As above mentioned, the deformation pattern can be considered as the result of the interaction between the main NNW–SSE regional compression and the local movements of the faults cutting the area. So, in a first step, we removed the effects of the motion of the Nubian plate with respect to the Eurasian plate, by estimating the movements at each GPS site adopting the Africa–Eurasia NUVEL-1A Eulerian pole (DeMets et al., 1994). As a final step, we inverted the residual velocity field adopting a Genetic Algorithm (Goldberg, 1989) optimization technique and assuming simple dislocation models (Okada, 1985). The inversion (hereinafter RSV) was performed through a simultaneous searching for three dislocation sources located between Vulcano and Lipari islands (S1), along the onshore of the Gulf of Patti (S2), and

in the Messina Strait (S3) respectively (Fig. 4). Based on field observations and previously published data (*e.g.* Ventura, 1994; Tortorici et al., 1995; Argnani et al., 2007; Giammanco et al., 2008; Mattia et al., 2008a), we fixed the position, the strike (the same as used for the vectorial decomposition approach), the depth of the top and the length for the S1 and the S2 sources. For the S3 sources we fixed the length, the depth of the top and constrained the strike to be within ~20° of the N30°E trend (*i.e.* parallel to the Messina Strait and perpendicular to the maximum extensional strain). The remaining parameters were searched through a blind inversion. Although the assumptions of the model (homogeneous, isotropic and elastic half-space with flat surface) represent an oversimplification of the actual conditions, this model is able to perform a good first-order modelling of the observed velocity field. In addition, we are aware that our results represent a sort of "average" of the "active" tectonic sources during the investigated period. Furthermore, the main results highlight some important aspects, closely connected to the kinematic of each sources (Table 2 and Fig. 4). S1 and S2 move as a dextral transpressive fault and a dextral transtensive fault respectively, with values of strike–slip and tensile component very close to those estimated by the vectorial decomposition approach. S3 moves as a normal fault and is characterized by a high dip–slip rate (about 15 mm/yr). So, in order to avoid bias due to the ambiguity of a fixed reference system we performed a new inversion (hereinafter BA) taking into account the GPS baselines and their length variations. We inverted each source separately searching for the opening, the strike– and the dip–slip components, while the remaining parameters were fixed to values inferred from RSV inversion. The results confirm the rates of movement, previously estimated for S1 and S2 sources and inferred a dip–slip rate of about 5 mm/yr for S3 source (Table 2 and Fig. 4). In light of this, it seems that the high dip–slip rate inferred for S3 source could be due to "residual effects" of Africa–Eurasia NUVEL-1A Eulerian pole, whereas S1 and S2 sources do not suffer this kind of effect. This suggests that the Messina Strait area and the southernmost Calabria motions significantly differ from the NNW–SSE plate convergence predicted for this area by large-scale crustal motion models (DeMets et al., 1994; Sella et al., 2002; Nocquet and Calais, 2004).

5. Discussions

In this work, we studied the deformation pattern along the western part of the Calabro-Peloritano Arc through 12 years of GPS measurements. Results highlight residual movements of the investigated area relative to Eurasia. The estimated strain-rate pattern clearly detects an area of a N–S shortening of about 0.65 µstrain/yr, coupled with an E–W extension of about 0.15 µstrain/yr between Vulcano and Lipari islands. Across the Nebrodi–Peloritani and the Messina Strait areas the strain-rate pattern is extensional, showing a NW–SE-oriented extension of about 0.15 µstrain/yr along both the MS and the ATL fault systems. These findings are generally consistent with the regional frame illustrated by geological, seismological and geodetic data published in literature (*e.g.* D'Agostino and Selvaggi, 2004; Neri et al., 2005; Billi et al., 2006; Ferranti et al., 2008a).

This deformation pattern can be considered as the result of the interaction between the main NNW–SSE regional compression and the local movements of the main faults cutting the area (*i.e.* ATL and MS

Fig. 1. a) Regional tectonic map of southern Italy. Focal mechanisms of earthquakes ($M \geq 3.5$; depth < 40 km) are selected from: Frepoli and Amato, 2000; Pondrelli et al., 2006; Neri et al., 2003, 2005; Musumeci et al., 2005; Giammanco et al., 2008; Harvard CMT solutions (http://www.seismology.harvard.edu). CPU, Calabro-Peloritano Arc Units; SMU, Sicilian–Maghrebian Units; V, Volcanic rocks; HFU, Hyblean Foreland Units; 1) main thrust front; 2) main faults; 3) contour of the subducted slab labelled in kilometres redrawn from D'Agostino and Selvaggi, 2004. b) Simplified tectonic map of north-eastern Sicily and southern Calabria redrawn from Lentini et al. (2000) and Monaco and Tortorici, (2000). ATL, Aeolian–Tindari–Letojanni fault system; MS, Messina Strait; PM, Peloritani Mts.; NM, Nebrodi Mts.; CM, Capo Milazzo. GPS stations analyzed in this work are so reported: 1) CGPS stations; 2) Peloritani–Nebrodi network; 3) Messina Strait network; and 4) Lipari–Vulcano network. Inset shows the IGS stations used in this work. Velocities computed for the 1996.00–2008.21 time interval are also shown. c) Zoom of the Lipari–Vulcano area. d) Zoom of the Messina Strait area. e) Horizontal velocity variations along the ABC profile. Velocity vectors have the same scale as sub-Fig. 1b.

Table 1
Site code, geodetic coordinates, observation history and east, north and up velocity components and associated errors are also reported for all GPS stations included in the processing.

Site	Long.	Lat.	1996	1997	1998	1999	2000	2001	2002	2003	2004	2005	2006	2007	2008	V_E mm/yr	V_N mm/yr	V_U mm/yr	Annotation
9518	15.01	37.95			I				I	I			I			−1.53±0.77	5.68±0.74	−1.50±1.06	SGPS
AJAC	8.76	41.93							██████		████					0.50±0.30	0.82±0.21	−0.24±0.47	IGS
CAGL	8.97	39.14	████████████████					███		███████						0.80±0.14	0.50±0.09	−0.19±0.26	IGS
CALA	14.92	38.18	I		I				I	I			I			−0.45±0.68	7.38±0.66	0.14±0.83	SGPS
9532	15.27	37.87	I		I				I	I			I			−1.41±0.71	4.28±0.68	2.35±1.11	SGPS
CPAN	15.08	38.64									██ ████ ██					4.70±1.04	5.15±0.94	−7.44±1.23	CGPS
FDNV	14.92	38.10							I	I			I			−0.78±1.08	3.68±1.04	−5.22±1.83	SGPS
FLOR	14.91	37.99							I	I			I			−2.95±1.11	2.14±1.05	−0.50±1.63	SGPS
GALL	15.29	37.92							I	I			I			−1.15±1.11	−1.24±1.05	−1.25±1.64	SGPS
GRAS	6.92	43.76	██ █████ ██ █					██████		██████████						0.74±0.15	0.73±0.11	0.91±0.27	IGS
GRAZ	15.49	47.07	████████████████████████													1.18±0.14	0.66±0.10	−0.21±0.27	IGS
LAMP	12.61	35.50				███████████				████████						−2.39±0.19	3.52±0.13	−0.96±0.31	IGS
LCAP	14.954	38.444	I I	I		I		I	I	I	I					−1.43±0.73	5.5±0.7	−10.45±1.08	SGPS
LFAL	14.945	38.444	I		I		I		I	I	I	I				−0.63±0.75	6.98±0.71	−11.66±1.07	SGPS
LGUA	14.946	38.455	I						I	I	I	I				−1.88±0.75	5.65±0.71	−18.45±1.14	SGPS
LMAZ	14.905	38.483	I I		I				I	I	I	I				0.87±0.72	4.96±0.69	−14.95±0.93	SGPS
LOSV	14.948	38.446		██▪ ██████					█	█████						−1.59±0.52	8.15±0.5	−18.18±0.61	CGPS
LROS	14.977	38.483	I I						I	I	I	I				−2.93±0.72	4.71±0.7	−11.01±1.16	SGPS
LSAN	14.934	38.485	I		I		I		I	I	I	I				−0.51±0.72	3.95±0.7	−14.78±1.08	SGPS
MAND	15.29	38.02	I		I				I							3.35±0.94	−0.62±0.89	−6.00±1.62	SGPS
MATE	16.70	40.65	████████████████████████													1.18±0.14	4.26±0.10	−0.05±0.26	IGS
MEDI	11.65	44.52	███████████████████████										▪ ██			2.15±0.15	1.83±0.10	−2.02±0.27	CGPS
MESS	15.55	38.21										████				2.08±1.19	3.06±1.05	−3.51±1.98	CGPS
MILA	15.23	38.27									▪▪████ ██					2.23±1.14	8.78±1.03	2.23±1.31	CGPS
MM01	15.50	38.17						I		I			I		I	0.64±0.30	3.38±0.22	−3.75±0.94	SGPS
MM04	15.55	38.24						I		I			I		I	0.46±0.33	2.61±0.24	−0.70±0.96	SGPS
MM06	15.63	38.26								I			I		I	0.67±0.58	4.42±0.43	−3.15±2.19	SGPS
MM08	15.68	38.24						I		I					I	1.19±0.32	3.20±0.23	−1.87±1.01	SGPS
MM09	15.70	38.22								I					I	0.36±0.56	2.78±0.42	−5.76±2.06	SGPS
MM10	15.64	38.23						I		I					I	−0.08±0.34	3.60±0.26	−1.91±1.15	SGPS
MM11	15.65	38.23						I		I					I	1.85±0.35	3.42±0.29	22.76±1.31	SGPS
MMME	15.25	37.94										██████				2.53±1.12	8.14±1.01	−1.81±1.26	CGPS
MNGR	15.18	37.95						I	I				I			−3.13±1.13	2.87±1.07	−0.61±1.86	SGPS
MONT	15.01	38.02	I		I				I	I			I			0.69±0.69	7.48±0.66	−2.71±0.79	SGPS
MPAZ	16.01	37.95											████			2.33±1.28	2.57±1.12	11.97±2.04	CGPS
MSRU	15.51	38.26										██████				0.48±1.16	4.51±1.04	−2.20±1.33	CGPS
MTTG	15.70	38.00										███ ▪▪				3.04±1.31	3.08±1.13	−1.66±2.06	CGPS
NOT1	14.99	36.88				███████████████										−1.23±0.19	4.78±0.12	−1.87±0.34	IGS
NOTO	14.99	36.88	██████ █████													−1.73±0.48	3.86±0.45	−2.09±0.60	IGS
NOVA	15.14	38.03						I	I				I			1.39±1.06	3.53±1.03	−2.50±1.44	SGPS
PACE	15.52	38.27						I	I				I		I	−0.84±0.94	3.24±0.92	6.95±1.34	SGPS
RODI	15.17	38.11						I	I				I			1.39±1.09	4.41±1.04	−1.57±1.43	SGPS
SPLA	15.49	38.08			I				I	I			I			0.38±0.96	3.53±0.93	1.75±1.21	SGPS
SPLB	15.22	38.81			▪██ ██		▪ ██		██████████							−0.25±0.51	2.56±0.49	−1.68±0.59	CGPS
SPLN	15.21	38.77			▪███ ███ ██		▪▪ ████████	███	▪▪ ██████							0.87±0.50	3.01±0.48	−1.42±0.61	CGPS
SPNC	15.35	38.15						I	I				I			−7.56±2.80	8.11±2.43	−1.86±6.18	SGPS

Table 1 (continued)

Site	Long.	Lat.	1996	1997	1998	1999	2000	2001	2002	2003	2004	2005	2006	2007	2008	V$_E$ mm/yr	V$_N$ mm/yr	V$_U$ mm/yr	Annotation
STDF	15.19	38.79														0.44±0.49	2.86±0.47	−1.25±0.55	CGPS
SVIN	15.23	38.80														0.30±0.77	3.41±0.71	−1.53±0.86	CGPS
TGRC	15.65	38.11														1.02±0.64	3.60±0.60	−0.34±0.73	CGPS
TIND	15.04	38.14														−1.62±0.69	7.34±0.66	4.66±0.88	SGPS
VCSP	14.952	38.409														1.54±0.55	8.02±0.53	−9.43±0.65	CGPS
VLEN	14.945	38.408														1.24±0.69	8.64±0.67	−8.44±0.87	SGPS
VMOL	14.986	38.396														−0.18±0.69	8.76±0.67	−7.9±0.91	SGPS
VPLI	14.956	38.430														−0.44±0.7	7.68±0.68	−10.88±0.95	SGPS
VROS	14.974	38.395														−1.17±1.31	8.79±1.16	−9.18±1.93	SGPS
VSAR	14.961	38.390														−0.92±0.71	9.88±0.68	−7.88±0.99	SGPS
VSER	14.985	38.378														−1.01±0.72	9.44±0.69	−5.46±1.04	SGPS
VVLC	14.961	38.426														−2.36±0.56	6.87±0.53	−9.77±0.7	SGPS
VCRA	14.965	38.403														−3.87±0.71	10.37±0.68	−12.31±0.94	SGPS
VLSG	15.64	38.22														2.92±1.14	5.82±1.02	0.41±1.30	CGPS
VVUL	14.963	38.426														−0.87±0.69	6.45±0.68	−10.59±0.94	CGPS

CGPS, permanent station; SGPS, sites surveyed in campaign-mode; IGS, permanent GPS station managed by International GNNS Service.

fault systems). While the main NNW–SSE regional compression is well constrained (*e.g.* DeMets et al., 1994; Sella et al., 2002; Nocquet and Calais, 2004), the knowledge of rate and deformation style across the ATL and the MS fault systems are poorly constrained. So, we adopted some different approaches to estimate the present-day deformation style across these faults. The main results highlight some important aspects, closely connected to the kinematic of each source (Table 2). S1 moves as a dextral transpressive fault in agreement with a sub-horizontal σ_1 NNE–SSW trending inferred from the inversion of focal mechanisms (Neri et al., 2005) and geological observations (Ventura, 1994), evidencing that the Lipari–Vulcano complex currently deforms in response to a dominant compressional stress field coexisting with a minor extensional component. S2 moves as a mainly dextral transtensive fault, in agreement with a near-vertical σ_1 together with $\sigma3$ trending ENE–WSW inferred from the inversion of focal mechanisms (Neri et al., 2005) and with the geological observations (Giammanco et al., 2008), depicting a prevailing "normal faulting" tectonic regime. The S1 and S2 sources are discrete segments of the ATL fault system that is considered by most investigators as part of a deep-seated lateral tear (STEP fault; *e.g.* Carminati et al., 1998, Govers and Wortel, 2005; Argnani et al., 2007), located close to Mt. Etna, Aeolian and Tyrrhenian Sea volcanoes and developing since 0.5–0.8 Ma (*i.e.* Goes et al., 2004). The inferred widths of S1 and S2 (3.5 and 5.1 km respectively) are scarcely consistent with the "lithospheric width" expected for a STEP fault. Considering that the age of the STEP fault is too young for a mature fault zone to have developed, S1 and S2 could be considered as structures reactivated in response to the local stress field.

S3 moves as a normal fault, in agreement with a vertical σ_1 and an ESE–WNW trending $\sigma3$ inferred from the inversion of focal mechanisms (Neri et al., 2005) and with geological observations (Tortorici et al., 1995), depicting a prevailing "normal faulting" tectonic regime. Several models have been proposed in literature for this area, in order to describe the fault responsible for the 1908 Messina Strait earthquake (see Amoruso et al., 2002 for an overview). The S3 source is scarcely consistent with the published sources. This should not be surprising, because i) the time intervals are different (all models consider the ground deformation pattern as due to a coseismic rupture, whereas our model refers to a short temporal window inside the inter-seismic period), and ii) as above mentioned, the S3 source represents a sort of "average" of the

"active" tectonic sources during the investigated period across the Messina Strait.

All these features clearly point to the presence of i) a compressional domain across the southernmost part of the Aeolian Archipelago, along a transpressive belt extending from Capo Milazzo to Salina (Mattia et al., 2008a), and ii) an extensional domain in north-eastern Sicily and southern Calabria. Within the regional tectonic context, these two different patterns are interpreted thus: the former is assumed as part of the main contractional belt located in the southern Tyrrhenian Sea, connected with the Nubia–Europe collision, and accommodated by geodetic convergence and seismological contraction between Sicily and Sardinia (e.g., Goes et al., 2004; Pondrelli et al., 2004; Serpelloni et al., 2005; Ferranti et al., 2008a) while the latter is ascribed to a rifting process along the NNE–SSW trending margins of western Calabria and north-eastern Sicily (Tortorici et al., 1995; Catalano et al., 2003), or to a counter-clockwise rotation of the Ionian block, resulting in normal faulting along the Tyrrhenian margin of Calabria and along the Ionian margin of Sicily (D'Agostino and Selvaggi, 2004). In any case, the ATL can be considered part of a diffuse transform boundary linking the active contractional belts in the Ionian and southern Tyrrhenian compartments (Doglioni et al., 2001; Billi et al., 2006; Ferranti et al., 2008a). Our data strongly support the hypothesis concerning a contractional domain extending from Capo Milazzo to Salina (S1 source), whereas they do not allow us to clearly discriminate among the models proposed for the extensional tectonics of southern Calabria and north-eastern Sicily (e.g. Amoruso et al., 2002; Valensise and Pantosti, 1992). However, geodetic data here presented significantly improve the spatial resolution of current tectonic strain-rate acting along the Calabro-Peloritano Arc.

6. Conclusions

The geodetic data presented in this work allowed constraining the present-day deformation pattern along the western part of the Calabro-Peloritano Arc. A marked decrease of velocity values from northern Sicily to the Aeolian islands can be recognized, showing how part of the NNW–SSE regional compression is localized within a ~15 km-wide zone with the buttressing of Vulcano and Lipari islands. This finding is of particular relevance because it extends to the east the
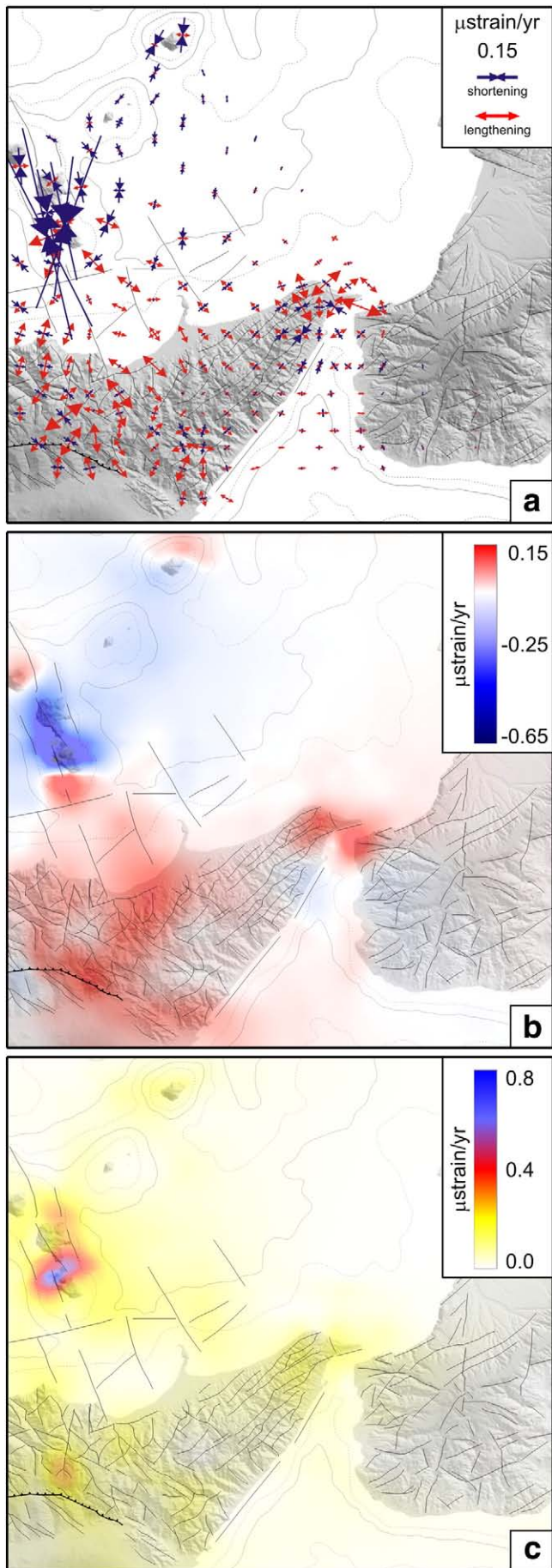
~E–W trending contractional belt with unprecedented resolution compared to the previously published studies (*e.g.* Hollenstein et al., 2003; D'Agostino and Selvaggi, 2004; Serpelloni et al., 2005).

Across the Nebrodi–Peloritani and the Messina Strait areas the strain-rate pattern is extensional, showing the maximum values along the MS and the ATL fault system. The analyses of velocities of selected stations allow estimating both the kinematics and rates of the ATL and the MS fault systems. In addition, these results were investigated through some simplified analytical models of the local tectonics, taking into account the regional context at a larger scale (Eurasia–Nubia convergence). The coherence between our results and the geological and seismological data available for the investigated area is an encouraging result. The large dataset used in this work is more accurate than those available for the past investigations (*e.g.* Hollenstein et al., 2003; Goes et al., 2004; D'Agostino and Selvaggi 2004; Argnani et al., 2007), thereby enabling improvements in the knowledge of this seismically hazardous area.

Acknowledgments

References

Altamimi, Z., Collilieux, X., Legrand, J., Garayt, B., Boucher, C., 2007. ITRF2005: a new release of the International Terrestrial Reference Frame based on time series of station positions and Earth Orientation Parameters. J. Geophys. Res. 112, B09401. doi:10.1029/2007JB004949.

Amoruso, A., Crescentini, L., Scarpa, R., 2002. Source parameters of the 1908 Messina Straits, Italy, earthquake from geodetic and seismic data. J. Geophys. Res. 107 (B4), 2080. doi:10.1029/2001JB000434.

Anzidei, M., Baldi, Bovini, C., Casula, G., Gandolfi, S., Riguzzi, F., 1998. Geodetic surveys across the Messina Straits (southern Italy) seismogenetic area. J. Geodyn. 25 (2), 85–97.

Argnani, A., Serpelloni, E., Bonazzi, C., 2007. Pattern of deformation around the central Aeolian Islands: evidence from multichannel seismics and GPS data. Terra Nova 19, 371-323.

Barberi, F., Gasparini, P., Innocenti, F., Villari, L., 1973. Volcanism of the southern Tyrrhenian Sea and its geodynamics implications. J. Geophys. Res. 78 (23), 5221–5232.

Barberi, F., Gandino, A., Gioncada, A., La Torre, P., Sbrana, A., Zenucchini, C., 1994. The deep structure of the Eolian Arc (Filicudi–Panarea–Vulcano sector) in light of gravimetric, magnetic and volcanological data. J. Volcanol. Geotherm. Res. 61, 189–206.

Billi, A., Barberi, G., Faccenna, C., Neri, G., Pepe, F., Sulli, A., 2006. Tectonics and seismicity of the Tindary Fault System, southern Italy: crustal deformations at the transition between ongoing contractional and extensional domains located above the edge of a subducting slab. Tectonics 25, 1–20.

Blewitt, G., Lavallee, D., 2002. Effect of annual signals on geodetic velocity. J. Geophys. Res. 107 (B7), 2145. doi:10.1029/2001JB000570.

Bonaccorso, A., 2002. Ground deformation of the southern sector of the Aeolian Islands volcanic arc from geodetic data. Tectonophysics 351, 181–192.

Carminati, E., Wortel, M.J.R., Spakman, W., Sabadini, R., 1998. The role of slab detachment processes in the opening of the Western-Central Mediterranean basins: some geological and geophysical evidence. Earth Planet. Sci. Lett. 160, 651–665 2002.

Catalano, S., De Guidi, G., Monaco, C., Tortorici, G., Tortorici, L., 2003. Long-term behaviour of the Late Quaternary normal faults in the Straits of Messina area (Calabrian arc): structural and morphological constraints. Quat. Int. 101–102, 81–91.

D'Agostino, N., Selvaggi, G., 2004. Crustal motion along the Eurasia–Nubia plate boundary in the Calabrian Arc and Sicily and active extension in the Messina Straits from GPS measurements. J. Geophys. Res. 109, B11402. doi:10.1029/2003TC001506.

Fig. 2. Strain-rate parameters: a) principal axes of strain-rate; b) dilatation strain-rate; and c) maximum shear strain-rate.
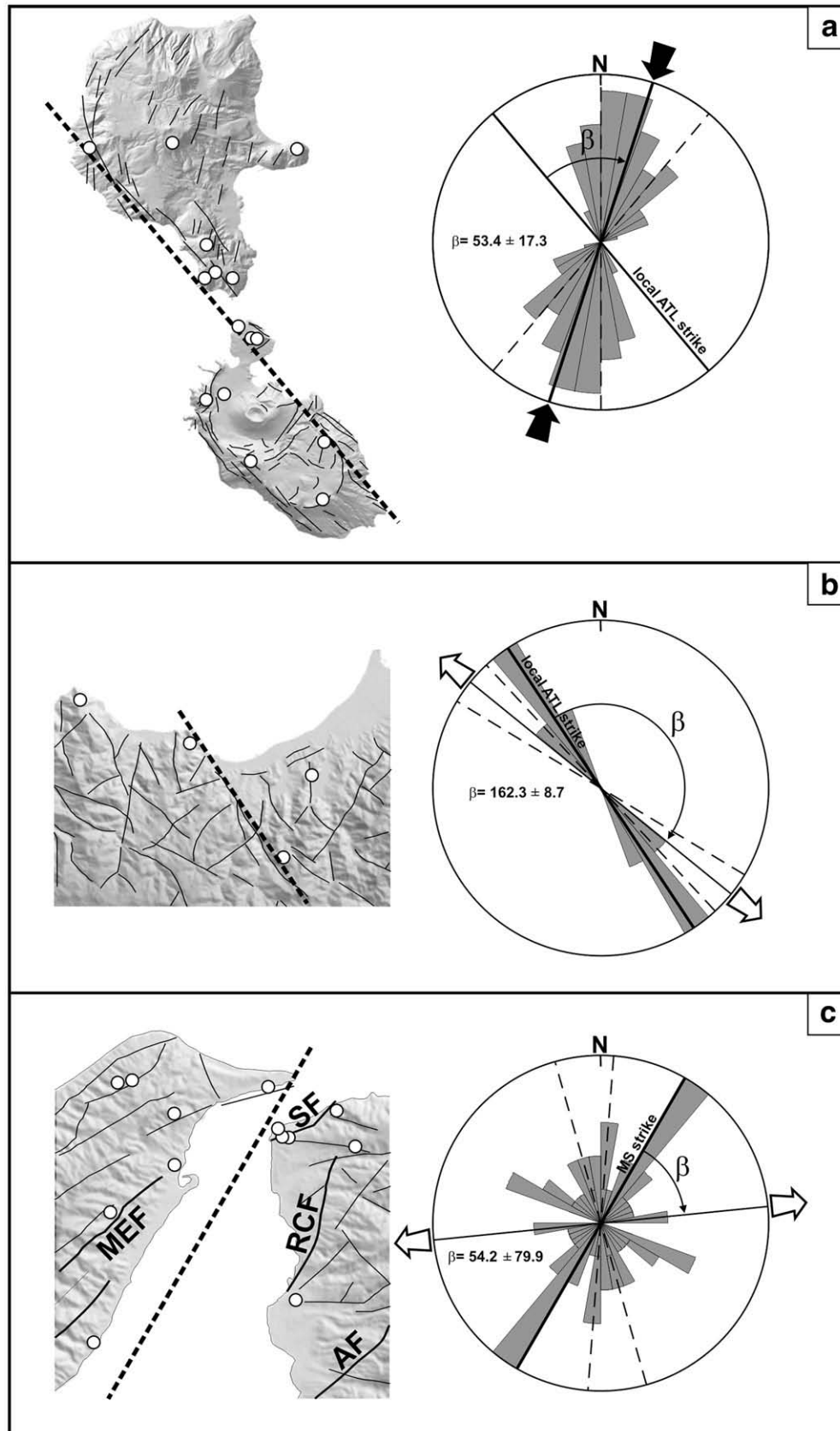
Fig. 3. Each map reports: on the left, a simplified structural tectonic sketch of the investigated sub-area, the network geometry used for the estimation of horizontal parallel and perpendicular movement rates on the selected fault (reported as a dashed line); on the right, a rose diagram showing the relationships between the vector displacement (resulting from the statistical approach explained in the text) and the local fault strike. The rose diagram also shows the azimuth value of each vector displacement computed for each pair of stations located across the analyzed fault. a) Analysis on the ATL sector cutting the Lipari-Vulcano islands: the fault moves as a dextral transpressive fault; b) Analysis on the ATL sector cutting the Gulf of Patti area: the fault moves as a dextral transtensive fault; c) Analysis on the MS fault system cutting the Messina Strait area: results are poorly constrained by the statistical approach. Active faults (redrawn from Ferranti et al., 2008b): AF, Armo fault; RCF, Reggio Calabria fault; MEF, Messina Fault; and SF Scilla fault.
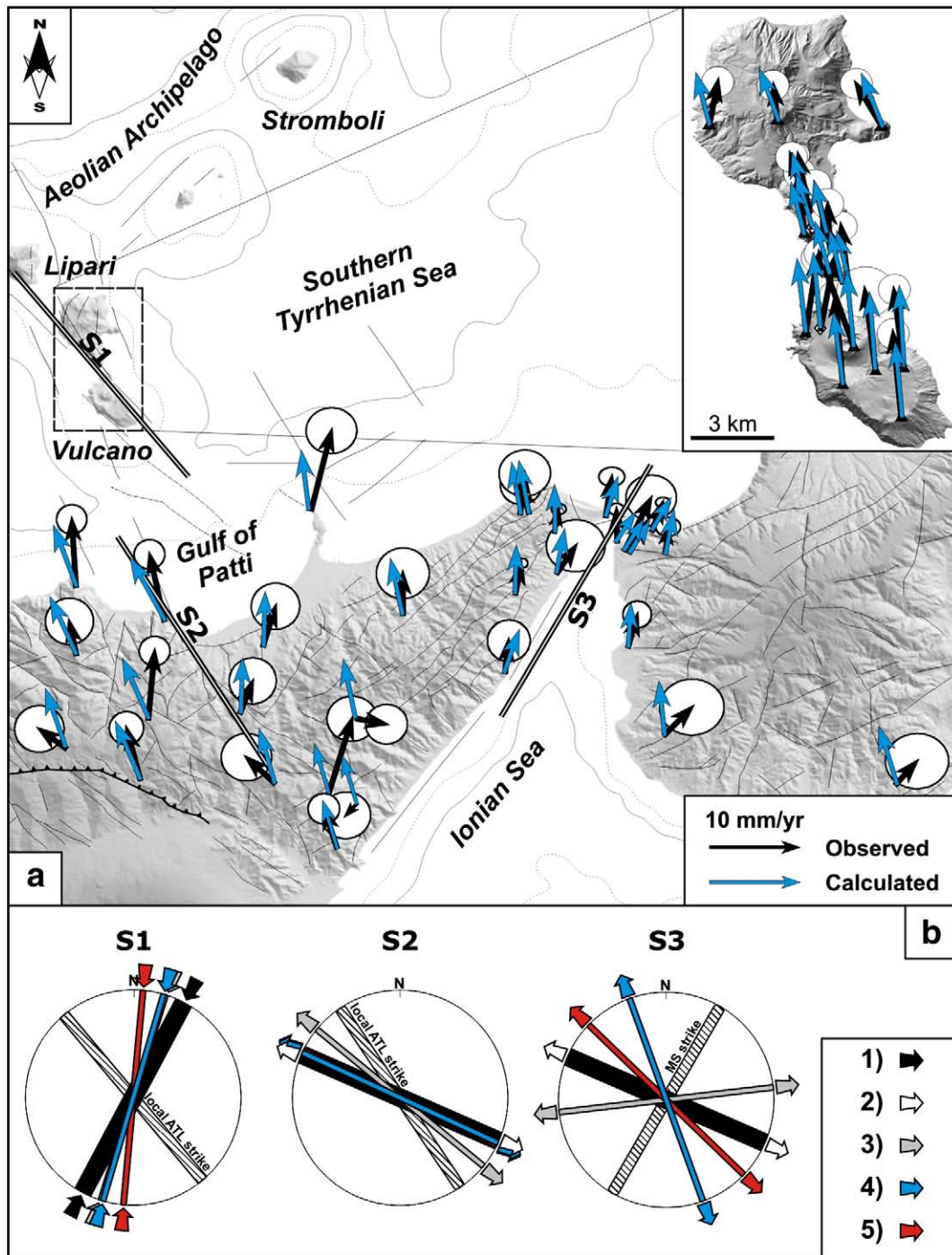
Fig. 4. a) Observed and calculated horizontal velocity vectors as resulting from the RSV inversion. Modelled sources S1, S2 and S3 are also reported. b) Geometric relationship among: 1) σ1 stress orientations; 2) σ3 stress orientations, and horizontal direction of slip inferred from 3) statistical approach; 4) RSV inversion and 5) BA inversion. The horizontal stress directions were derived from inversion of focal mechanisms (Neri et al., 2005).

Table 2
Parameters of the modelled sources for the 1996.00–2008.21 time interval.

Inversion model	S1		S2		S3	
	RSV	BA	RSV	BA	RSV	BA
Longitude (km)	495.90*	495.90#	505.50*	505.50#	550.00 ± 0.3	550.00#
Latitude (km)	4253.70*	4253.70#	4218.00*	4218.00#	4222.00 ± 0.3	4222.00#
Azimuth	N40°W*	N40°W#	N35°W*	N35°W#	N30°E ± 10	N30°E#
Depth (km)	0.0 b.s.l.*	0.0 b.s.l.#	0.0 b.s.l.*	0.0 b.s.l.#	0.0 b.s.l.*	0.0 b.s.l.#
Length (km)	40.00*	40.00#	40.00*	40.00#	40.00*	40.00#
Width (km)	4.54 ± 1.8	4.54#	5.10 ± 1.5	5.10#	7.80 ± 0.5	7.80#
Dip	81.90 ± 7.5	81.90#	75.60 ± 7.0	75.60#	80.10 ± 4.1	80.10#
Strike–slip (mm/yr)	− 2.2 ± 1.5	− 2.0 ± 0.4	− 3.1 ± 1.5	− 5.6 ± 1.7	− 1.1 ± 1.2	0.3 ± 0.3
Dip–slip (mm/yr)	− 5.6 ± 3.0	− 5.7 ± 0.5	4.1 ± 2.2	3.6 ± 2.1	− 15.3 ± 2.7	− 5.2 ± 1.2
Opening (mm/yr)	− 3.3 ± 2.2	− 2.0 ± 0.4	1.9 ± 1.3	3.5 ± 1.2	1.3 ± 0.8	1.2 ± 0.2

The RSV model uses as input the residual stations velocity with respect to the Africa–Eurasia NUVEL-1A Eulerian pole (DeMets et al., 1994); the BA model uses as input the GPS baselines and their length variations. Coordinates are WGS84–UTM 33N. *Values fixed to field observations and previously published data: see text for details. #Values fixed to RSV solution. Since solutions obtained by Genetic Algorithm optimization technique are affected by uncertainties due both to the uncertainties displacement measurements and uncertainties of the searching algorithm itself, for each parameter, errors were estimated by adopting a Jackknife re-sampling method (Efron, 1982).

De Astis, G., Ventura, G., Vilardo, G., 2003. Geodynamic significance of the Aeolian volcanism (Southern Tyrrhenian Sea, Italy) in light of structural, seismological, and geochemical data. Tectonics 22 (4), 1040. doi:10.1029/2003TC001506.

DeMets, C., Gordon, R.G., Argus, D.F., Stein, S., 1994. Effect of recent revisions to the geomagnetic reversal time scale on estimates of current plate motions. Geophys. Res. Lett. 21, 2191–2194.

Doglioni, C., Innocenti, F., Mariotti, G., 2001. Why Mt Etna? Terra Nova 13, 25–31.

Efron, B., 1982. The jackknife, bootstrap and other resampling plans, CBMS-NSF Series, Society for Industrial and Applied Mathematics, Philadelphia.

Esposito A., 2007. Studio della deformazione geodetica delle Isole Eolie con particolare riferimento all'Isola di Panarea. PhD Thesis, University of Bologna, pp. 137.

Faccenna, C., Becker, T.W., Lucente, F.P., Jolivet, L., Rossetti, F., 2001. History of subduction and back-arc extension in the Central Mediterranean. Geophys. J. Int. 145, 809–820.

Ferranti, L., Oldow, J.S., D'Argenio, B., Catalano, R., Lewis, D., Marsella, E., Avellone, G., Maschio, L., Pappone, G., Pepe, F., Sulli, A., 2008a. Active deformation in Southern Italy, Sicily and southern Sardinia from GPS velocities of the Peri-Tyrrhenian Geodetic Array (PTGA). Boll. Soc. Geol. Ital. (Ital. J. Geosci.) 127/2, 299–316.

Ferranti, L., Monaco, C., Morelli, D., Antonioli, F., Maschio, L., 2008b. Holocene activity of the Scilla Fault, Southern Calabria: insights from coastal morphological and structural investigations. Tectonophysics 453, 74–93. doi:10.1016/j.tecto.2007.05.006.

Frepoli, A., Amato, A., 2000. Spatial variation in stresses in peninsular Italy and Sicily from background seismicity. Tectonophysics 317, 109–124.

Ghisetti, F., Vezzani, L., 1982. Different styles of deformation in the Calabrian arc (southern Italy): implications for a seismotectonic zoning. Tectonophysics 85, 149–165.

Giammanco, S., Palano, M., Scaltrito, A., Scarfì, L., Sortino, F., 2008. Possible role of fluid overpressure in the generation of earthquake swarms in active tectonic areas: the case of the Peloritani Mts. (Sicily, Italy). J. Volcanol. Geotherm. Res. 178, 795–806. doi:10.1016/j.jvolgeores.2008.09.005.

Goes, S., Giardini, D., Jenny, S., Hollenstein, C., Kahle, H.G., Geiger, A., 2004. A recent tectonic reorganization in the south-central Mediterranean. Earth Planet. Sci. Lett. 226, 335–345.

Goldberg, D.E., 1989. Genetic Algorithms in Search, Optimization & Machine Learning. InAddison-Wesley, p. 372.

Govers, R., Wortel, M.J.R., 2005. Lithosphere tearing at STEP faults: response to edges of subduction zones. Earth Planet. Sci. Lett. 236, 505–523.

Gueguen, E., Doglioni, C., Fernandez, M., 1998. On the post-25 Ma geodynamic evolution of the western Mediterranean. Tectonophysics 298, 259–269.

Gvirtzman, Z., Nur, A., 2001. Residual topography, lithospheric structure and sunken slabs in the central Mediterranean. Earth Planet. Sci. Lett. 187, 117–130.

Haines, A.J., Holt, W.E., 1993. A procedure for obtaining the complete horizontal motions within zones of distributed deformation from the inversion of strain rate data. J. Geophys. Res. 98, 12,057–12,082.

Haines, A.J., Jackson, A., Holt, W.E., Agnew, D.C., 1998. Representing distributed deformation by continuous velocity fields. Sci. Rept. 98/5. In: Inst. of Geol. and Nucl. Sci. Wellington, New Zeland.

Herring, T.A., King, R.W., McKlusky, S.C., 2006a. GAMIT reference manual: GPS analysis at MIT, Version 10.3. Massachusetts Institute of Technology, Cambridge, M.A.

Herring, T.A., King, R.W., McKlusky, S.C., 2006b. GLOBK reference manual: Global Kalman filter VLBI and GPS analysis program, version 10.3. Massachusetts Institute of Technology, Cambridge, MA.

Hollenstein, Ch., Kahle, H.G., Geiger, A., Jenny, S., Goes, S., Giardini, D., 2003. New GPS constraints on the Africa–Eurasia plate boundary zone in southern Italy. Geophys. Res. Lett. 30 (18), 1935. doi:10.1029/2003GL017554.

Lentini, F., Catalano, S., Carbone, S., 2000. Carta geologica della Provincia di Messina, SELCA, Florence, Italy.

Malinverno, A., Ryan, W.B.F., 1986. Extension in the Tyrrhenian Sea and shortening in the Apennines as result of arc migration driven by sinking of the lithosphere. Tectonics 5, 227–245.

Mattia, M., Aloisi, M., Amore, M., Bonforte, A., Calvagna, F., Cantarero, M., Consoli, O., Consoli, S., Palano, M., Puglisi, B., Puglisi, G., Rossi, M., 2006. Monitoraggio geodetico delle deformazioni del suolo in area sismogenetica: la rete GPS dello Stretto di Messina. Quaderni di Geofisica 42, 20.

Mattia, M., Palano, M., Bruno, V., Cannavò, F., Bonaccorso, A., Gresta, S., 2008a. Tectonic features of the Lipari–Vulcano complex (Aeolian archipelago, Italy) from 10 years (1996–2006) of GPS data. Terra Nova 20, 370–377. doi:10.1111/j.1365-3121.2008.00830.

Mattia, M., Aloisi, M., Di Grazia, G., Gambino, S., Palano, M., Bruno, V., 2008b. Geophysical investigations of the plumbing system of Stromboli volcano (Aeolian Islands, Italy). J. Volcanol. Geotherm. Res. doi:10.1016/j.jvolgeores.2008.04.022.

Monaco, C., Tortorici, L., 2000. Active faulting in the Calabrian arc and eastern Sicily. J. Geodyn. 29, 407–424.

Musumeci, C., Patanè, D., Scarfì, L., Gresta, S., 2005. Stress directions and shear-wave anisotropy: observations from local earthquakes in Southeastern Sicily, Italy. Bull. Seismol. Soc. Am. 95 (4), 1359–1374.

Neri, G., Barberi, G., Orecchio, B., Mostaccio, A., 2003. Seismic strani and seismogenic stress regimes in the crust of the southern Tyrrhenian region. Earth Planet. Sci. Lett. 213, 97–112.

Neri, G., Barberi, G., Oliva, G., Orecchio, B., 2005. Spatial variations of seismogenetic stress orientations in Sicily, south Italy. Phys. Earth Planet. Inter. 148, 175–191.

Nocquet, J.M., Calais, E., 2004. Geodetic measurements of crustal deformation in the western Mediterranean and Europe. Pure Appl. Geophys. 161, 661–682.

Okada, Y., 1985. Surface deformation due to shear and tensile faults in a half-space. Bull. Seismol. Soc. Am. 75, 1135–1154.

Patacca, E., Sartori, R., Scandone, P., 1990. Tyrrhenian basin and Apenninic arcs. Kinematic relations since late Tortonian times. Mem. Soc. Geol. Ital. 45, 425–451.

Pondrelli, S., Piromallo, C., Serpelloni, E., 2004. Convergence vs. retreat in Southern Tyrrhenian Sea: insights from kinematics. Geophys. Res. Lett. 31, L06611. doi:10.1029/2003GL019223.

Pondrelli, S., Salimbeni, S., Ekström, G., Morelli, A., Gasperini, P., Vannucci, G., 2006. The Italian CMT dataset from 1977 to the present. Phys. Earth Planet. Inter. 159, 286–303.

Sella, G.F., Dixon, T.H., Mao, A., 2002. REVEL: a model for recent plate velocities from space geodesy. J. Geophys. Res. 107. doi:10.1029/2000JB000033.

Selvaggi, G., 2001. Strain pattern of the Southern Tyrrhenian slab from moment tensors of deep earthquakes: implications on the down–dip velocity. Ann. Geofis. 44 (1), 155–165.

Selvaggi, G., Chiarabba, C., 1995. Seismicity and P-wave velocity image of the Southern Tyrrhenian subduction zone. Geophys. J. Int. 121, 818–826.

Serpelloni, E., Anzidei, M., Baldi, P., Casula, G., Galvani, A., 2005. Crustal velocity and strain-rate fields in Italy and surrounding regions: new results from the analysis of permanent and non-permanent GPS networks. Geophys. J. Int. 161, 861–880.

Tortorici, L., Monaco, C., Tansi, C., Cocina, O., 1995. Recent and active tectonics in the Calabrian Arc (southern Italy). Tectonophysics 243, 37–55.

Valensise, G., Pantosti, D., 1992. A 125 Kyr-long geological record of seismic source repeatability: the Messina Straits (southern Italy) and the 1908 earthquake (Ms 7 1/2). Terra Nova 4, 472–483.

Valensise, G., Pantosti, D., 2001. Database of potential sources for earthquakes larger than M5.5 in Italy. Ann. Geofis. 44 (4) suppl. 180 pp.

Ventura, G., 1994. Tectonics, structural evolution and caldera formation on Vulcano Island (Aeolian Archipelago, southern Tyrrhenian Sea). J. Volcanol. Geotherm. Res. 60, 207–224.